Experimental and numerical studies of circular precast concrete slender columns with intermediate connection filled with high-performance concrete

Structures 57 (2023) 105204

Contents lists available at ScienceDirect

Structures

journal homepage: www.elsevier.com/locate/structures

Experimental and numerical studies of circular precast concrete slender columns with intermediate connection filled with high-performance concrete

Ahmed A. Hamoda [a], Mizan Ahmed [b], Aref A. Abadel [c], Mohamd Ghalla [a], Vipulkumar Ishvarbhai Patel [d], Qing Quan Liang [e,*]

[a] Department of Civil Engineering, Faculty of Engineering, Kafrelsheikh University, Kafrelsheikh, Egypt
[b] Centre for Infrastructure Monitoring and Protection, School of Civil and Mechanical Engineering, Curtin University, Kent Street, Bentley, WA 6102, Australia
[c] Department of Civil Engineering, College of Engineering, King Saud University, Riyadh 11421, Saudi Arabiad
[d] School of Computing, Engineering and Mathematical Sciences, La Trobe University, Bendigo, VIC 3552, Australia
[e] College of Sport, Health, and Engineering, Victoria University, PO Box 14428, Melbourne, VIC 8001, Australia

ARTICLE INFO

Keywords:
Precast concrete column
Slender columns, High-performance concrete
Finite element modeling

ABSTRACT

Precast concrete (PC) slender columns with intermediate connections are often used in building construction. However, no studies have been performed on the behavior of PC slender columns with intermediate connections filled with high-performance concrete namely engineering cementitious composites (ECC) and strain hardening cementitious composites (SHCC). This paper presents the testing and computer modeling of axially loaded PC slender columns with splices filled with ECC and SHCC. Experimental program and results are presented on nineteen PC slender columns under concentric compressive load up to collapse. The test parameters include the longitudinal reinforcement (μ) ratio, and embedded length of steel bars/infilled concrete connection (L_e). Three different reinforcement ratios of 0.027, 0.031, and 0.036 are considered. The embedded length of steel bars/intermediate concrete connection varies from 15D, 22.5D, and 30D where D is the bar diameter. Experimental results indicate that the use of longer steel bars/intermediate concrete connection and a higher reinforcement ratio can significantly enhance both the cracking and ultimate loads of PC slender columns with an intermediate concrete connection. The elastic stiffness of the PC slender columns with ECC and SHCC connection is found to increase by 150% and 93%, respectively when compared to the control specimen. Similarly, filling the splice of the PC columns with ECC and SHCC improves the energy absorption capacity by 107% and 138%, respectively. Nonlinear three-dimensional finite element models (FEMs) are developed accounting for the initial imperfection of the slender columns and their accuracy is validated by experimental results. It is shown that the FEM can provide an accurate simulation of the performance of PC columns with splice connection.

1. Introduction

Reinforced Concrete (RC) columns are widely used in constructing multi-story buildings, car parks, shopping malls, and bridge piers. However, in-situ RC columns require significant onsite activities such as the preparation of formwork, reinforcement placement, and casting concrete followed by curation for a few days. In addition, delivering materials and heavy equipment to the sites can increase the carbon emission for a specific project [1]. To significantly reduce carbon emissions, alternative construction materials and prefabricated structural components should be used in the construction of infrastructure. Precast Concrete (PC) columns are cast in a prefabricated environment, which reduces the onsite activities. As a result, the use of PC columns in structures significantly reduces the construction costs and carbon footprint [2]. However, considering the restriction on transportation length, PC columns with only a limited length can be delivered to the site. Multiple PC columns then need to be connected to achieve the desired length. Moreover, the use of column splices is often required by the site erection condition rather than the structural needs.

Extensive studies were performed to investigate the structural performance of traditional RC columns [3–6]. Previous studies showed that the performance of RC columns is governed by the reinforcement ratio of

* Corresponding author at: College of Sport, Health, and Engineering, Victoria University, PO Box 14428, Melbourne VIC 8001, Australia.
E-mail address: Qing.Liang@vu.edu.au (Q.Q. Liang).

https://doi.org/10.1016/j.istruc.2023.105204
Received 16 July 2023; Received in revised form 28 August 2023; Accepted 5 September 2023
Available online 19 September 2023

longitudinal and transverse reinforcement. Depending on the size and applied loads, the failure modes of RC columns include the crushing of cover concrete, the buckling of reinforcing bars, bending, and combined failure modes [7,8]. During the earthquakes occurred in 2008 in Wenchuan, China, and Tōhoku, Japan in 2011, the columns commonly failed by flexure [9]. The flexural collapse of RC columns may be caused by the reduction in their ductility and flexural strength. Some studies were carried out in order to enhance the flexural performance of such columns [10,11]. Hong et al. [12] investigated experimentally the seismic behaviors of RC columns considering buckling. The effect of slenderness ratios was examined. It was concluded that increasing the slenderness ratio increased the displacements of the columns resulting from global buckling. Recently, research studies on PC columns and their connections were undertaken by researchers. Xu et al. [2] carried out tests on PC columns to study the effect of concrete strengths, rebar layouts, and axial loads on their fire performance. Test results showed that the fire resistance of PC columns was significantly impacted by the axial load applied. The columns made of lower-strength concrete had a better fire performance than the columns made of High Strength Concrete (HSC). Robinson [13] studied the effects of concrete mixes comprising lightweight aggregates on the responses of PC columns subjected to horizontal and vertical loads. Beni and Madhkhan [14] performed tests on PC beam-column connections subjected to seismic loading. They proposed connections with steel profiles as corbels with high-strength structural bolts to eliminate in-situ concrete casting. However, their test results showed that the proposed precast connections had higher strength and stiffness degradation than the in-situ connections.

Nowadays, High-Performance Concrete (HPC) is increasingly used to replace Normal Concrete (NC) to improve the load-bearing capacity and tensile properties of concrete [15]. Engineering Cementitious Composites (ECC) and Strain Hardening Cementitious Composites (SHCC) are two kinds of HPC. The ECC and SHCC usually presents a strain-hardening performance after the occurrence of the first crack instead of the rapid softening and collapse often observed in NC [16]. It has been found that ECC and SHCC have higher flexural and tensile strengths and ductility than the NC [17–22]. In addition, the enhanced ductile characteristic of ECC and SHCC improves the bond strength between the concrete and reinforcing bars. Moreover, ECC and SHCC reduces the width of cracks; thus it may prevent corrosion and associated deterioration of concrete [23]. It has also been found that the use of ECC and SHCC in structural members can improve the flexural characteristics, ductility, and failure mode of structural elements [17–19]. The performance of RC columns made of ECC under axial loading was studied experimentally by Emara et al. [24]. Sixteen circular columns were tested to capture the improvement in the crack pattern, ultimate capacity, and durability of the RC columns compared to NC columns. It was found that ECC columns with 1.5% polypropylene fiber had the highest ultimate compressive strength, superior durability, and maximum ductility. Qian et al. [25] carried out an experimental investigation on RC bridge columns integrated with the ECC segment at the plastic zone under cyclic loading. The results showed that the behavior of ECC columns was improved when compared with NC columns. Spalling of ECC did not appear in the whole loading stages. Shuai et al. [26] examined the mechanical performance of ECC-HSC stub columns under axial compressive loading and developed finite element models for such columns. The results showed that the circumferential stress and radial stress in the ECC ring were not uniform in different zones. Increasing the ECC ratio higher than the HSC can improve the ultimate load. Baraghith et al [27] caried out an experimental investigation on improving the shear behavior of RC dapped-end beams using precast SHCC plates. The test results revealed that providing RC beams with precasted SHCC plates could significantly enhance both the shear capacity and ductility. Esmaeeli and He [28] studied the cast-in-situ and prefabricated solution with SHCC for seismic retrofitting of severely damaged substandard RC beam-column joints. The experimental results revealed that the bond between the retrofitting system and the concrete plays a determining role in the performance of the proposed techniques. Recently, Hamoda et al. [29] tested PC beams with intermediate connection under flexural load. It was found that increasing the reinforcement ratio and the embedded length improved the flexural performance of the PC beams with intermediate connections.

The literature review shows that limited studies have been performed to study the behavior of PC columns connected with ECC and SHCC connections. However, no investigation has been reported on the effects of the longitudinal reinforcement ratio and the length of column splices on the responses of PC slender columns. Moreover, the sensitivity of the structural performance of PC slender columns to the strain hardening of cementitious materials has not been examined experimentally. Thus, this paper fills these knowledge gaps by investigating the axial performance of circular PC slender columns with ECC and SHCC intermediate connections. Nineteen full-scale circular columns with various longitudinal reinforcement (μ) ratio and embedded length (L_e) of steel bars or splice connection were tested under compression up to collapse. The experimental program is presented, and the test results are discussed. FEM is developed using ABAQUS and the accuracy of the nonlinear simulations is verified against the experimental results.

2. Experimental program

2.1. Specimen details and test program

Nineteen circular PC slender columns were constructed and tested under axial compressive force up to collapse. To compare the enhancement of the performance of PC slender columns with a different type of intermediate concrete connections, one normal RC slender column with identical geometry and without an intermediate connection was also tested which was considered as the control specimen as shown in Fig. 1.

All columns were designed to have the same diameter of 150 mm and total height of 1700 mm. It should be noted that the columns consisted of three parts; two of them were precast NC parts connected by ECC or SHCC, as shown in Fig. 1. Closed ring steel stirrups with a diameter of 8 mm and 185 mm spacing were used for all specimens. Two parameters were considered in this study including the reinforcement ratio of the longitudinal steel bars (μ), and the embedded length of steel bars/ intermediate concrete connection (L_e). Columns were divided into three groups for ECC and SHCC concrete types according to the reinforcement ratio, as shown in Table 1. Columns in Group G1, G2, and G3 had a reinforcement ratio of 0.027, 0.031, and 0.036, respectively. For each group, columns with three different embedded lengths of 15D, 22.5D, and 30D were tested, in which D is the bar diameter. In the naming of the columns, 'E' represents ECC, and 'H' represents SHCC concrete type, the 2nd number represents the reinforcement ratio, and the 3rd number represents the embedded length of steel bars/ intermediate concrete connection.

2.2. Casting and preparation of tested columns

As shown in Fig. 2 (a), cylindrical plastic formworks were used in vertical positions to form the two PC panels for each column. The precast NC columns were constructed, as shown in Fig. 1 (a) with appropriated height L_1 of 775 mm, 737.5 mm, and 700 mm, mentioned in Table 1, with the additional length for splices L_e of 15D, 22.50, and 30D. To make a full-length column, two precast NC columns with the same L_1 were connected oppositely leaving a space (L_e) to cast ECC/SHCC inside, giving the total length of 1700 mm, as shown in Fig. 2 (b,c). For example, two NC panels with $L_1 = 775$, 737.50, and 700 mm connected with $L_e = 150$, 225, and 300, respectively, provided the total length of the columns as 1700 mm.

The ECC/SHCC connection between the NC precast columns was formed with a plastic cylinder containing an opening in the upper part, as shown in Fig. 2 (b, c) to cast the flowable ECC inside. The two NC

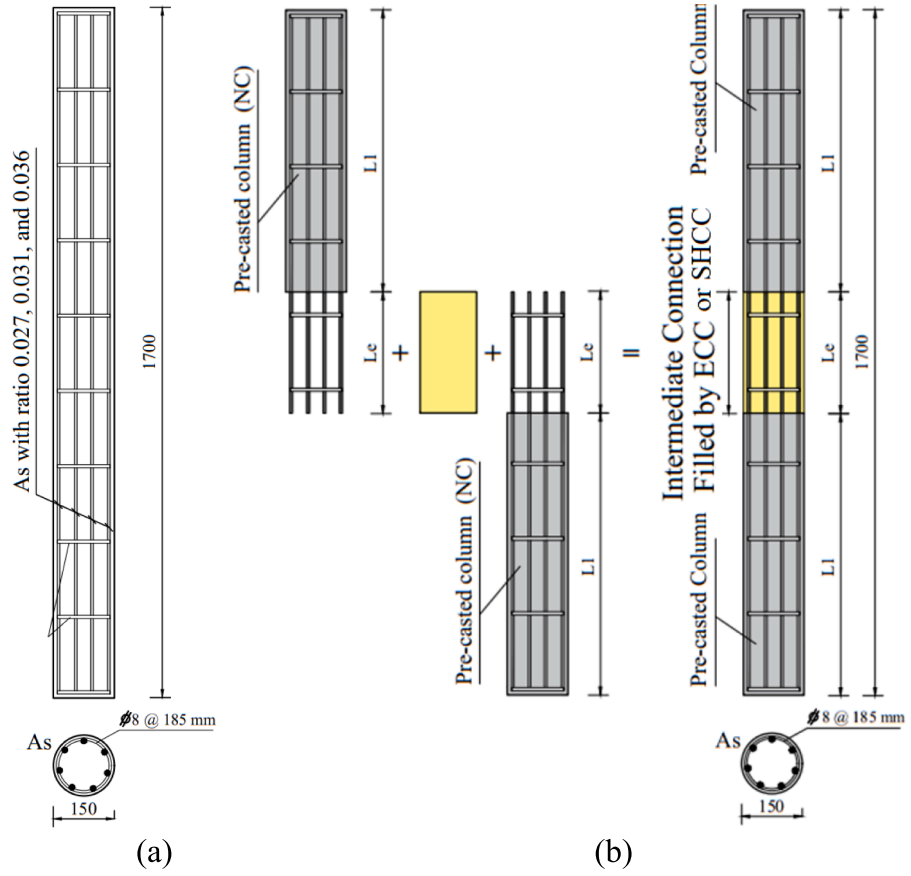

Fig. 1. Geometric and reinforcement details of the columns: (a) control specimen, $C_{0,}$ and (b) Precast RC columns with ECC/SHCC connection. (Units: mm).

Table 1
Test Matrix.

Group	Column's ID	Concrete type	Embedded Length (L_e)	L1 (mm)	Longitudinal steel with (μratio)
ECC group					
G1-ECC	C_0	NC	———	———	6#10 mm (0.027)
	E-0.027–15	ECC	15D	775.0	
	E-0.027–22.5	ECC	22.5D	737.5	
	E-0.027–30	ECC	30D	700.0	
G2-ECC	C_0	NC	———	———	6#10 mm (0.027)
	E-0.031–15	ECC	15D	775.0	7#10 mm (0.031)
	E-0.031–22.5	ECC	22.5D	737.5	
	E-0.031–30	ECC	30D	700.0	
G3-ECC	C_0	NC	———	———	6#10 mm (0.027)
	E-0.036–15	ECC	15D	775.0	8#10 mm (0.036)
	E-0.036–22.5	ECC	22.5D	737.5	
	E-0.036–30	ECC	30D	700.0	
SHCC group					
G1-SHCC	C_0	NC	———	———	6#10 mm (0.027)
	H-0.027-15D	SHCC	15D	775.0	
	H-0.027–22.5D	SHCC	22.5D	737.5	
	H-0.027-30D	SHCC	30D	700.0	
G2-SHCC	C_0	NC	———	———	6#10 mm (0.027)
	H-0.031-15D	SHCC	15D	775.0	7#10 mm (0.031)
	H-0.031–22.5D	SHCC	22.5D	737.5	
	H-0.031-30D	SHCC	30D	700.0	
G3-SHCC	C_0	NC	———	———	6#10 mm (0.027)
	H-0.036-15D	SHCC	15D	775.0	8#10 mm (0.036)
	H-0.036–22.5D	SHCC	22.5D	737.5	
	H-0.036-30D	SHCC	30D	700.0	

L_e: Embedded length; **E**: ECC; **H**: SHCC; **D**: Bar diameter; **L1:** Precast column length.

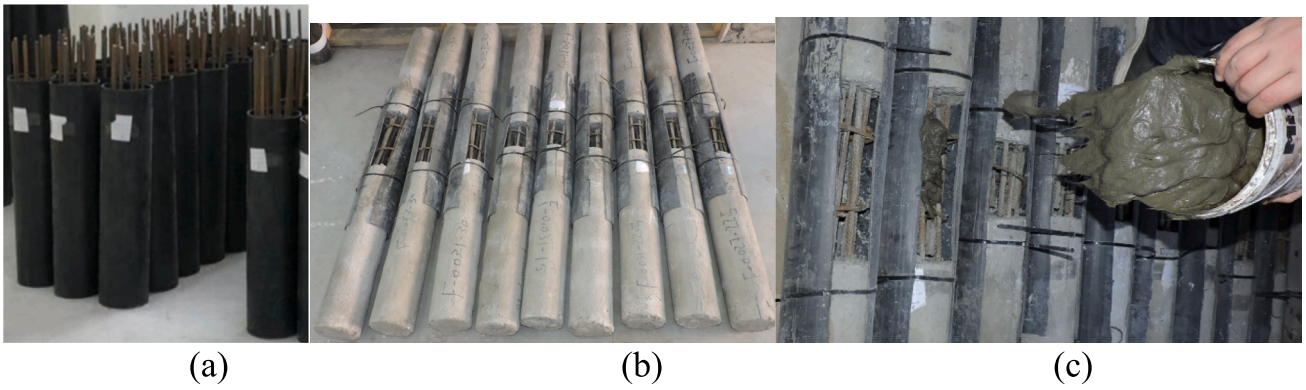

Fig. 2. Casting and preparation: (a) The plastic cylinder formwork, (b) Connecting the precast NC panels considering L_e, and (c) Casting of the construction joint.

panels were painted white, while the ECC/SHCC connection was unpainted to identify the interface surfaces.

2.3. Material properties and mix proportion

Ready mix NC and ECC/SHCC with mix proportion shown in Table 2 were used to cast the specimens. It can be seen from Table 2 that the ECC requires a higher cement quantity and high range water reducer (HRWR) compared to SHCC. Therefore, from economical point of view, SHCC is preferable to be used to fill the splice connection of the precast columns. The compression tests on three standard cylinders of 150 mm diameter and 300 mm height were conducted on the same day of testing of the columns. The compressive strengths of both types of concrete were measured and are presented in Table 2. As shown in Fig. 3, uniaxial tensile tests were carried out on dog-bone concrete specimens according to the recommendations specified by ACI [30]. The concrete tensile strengths of NC, ECC and SHCC were estimated experimentally as about 2.61 MPa, 4.58 MPa and 4.82 MPa, respectively. The uniaxial stress–-strain laws for NC, ECC and SHCC calibrated and adapted based on tests shown in Fig. 4. Tensile coupon test was performed to determine the mechanical properties of the used steel elements. The yield stress of the steel bars with 8 mm and 10 mm bars was measured as 270 MPa and 397 MPa, respectively. The tensile stress of the steel bars with 8 mm and 10 mm bars was measured as 513 MPa and 594 MPa, respectively. The measured stress–strain curves of steel bars are shown in Fig. 5.

2.4. Loading arrangement, test setup, and instrumentation

The experimental program was carried out at Kafrelsheikh University, Egypt. The axial compression force was applied on the circular PC slender column using a hydraulic jack with 1000 kN capacity fixed at the rigid steel frame, as shown in Fig. 6. All columns were tested with identical boundary conditions. The boundary condition was chosen to be as roller support at the column‘s top allowing only the vertical jack movement, while it was hinged at the column‘s bottom surface, as shown in Fig. 6.

Two solid steel balls were designed to achieve point loads on both ends of the columns as shown in Fig. 6 (b). In order to avoid the premature failure that may occur at the columns‘ ends, thick circular steel tubes were used to jacket the two columns‘ ends close to the loading

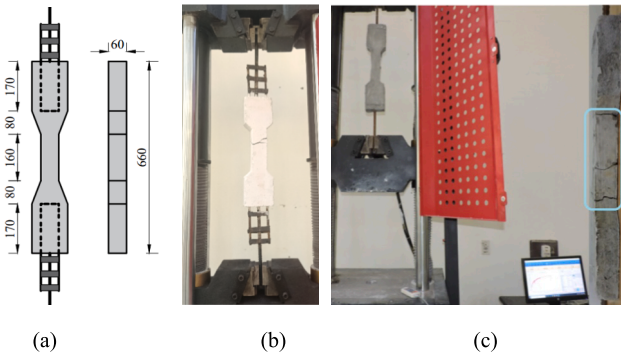

Fig. 3. Uniaxial tensile test: (a) Concrete specimen dimensions, (b) cracking of NC, and (c) Cracking of ECC.

regions. Eight Linear Variable Displacement Transducers (LVDT) were positioned surrounding the column‘s mid-height as shown in Fig. 6(b). All sensors were then connected to the data logger system to automatically register the recordings during the experimentation, as shown in Fig. 6 (c).

3. Test results and discussion

3.1. Crack pattern and failure modes

The cracking load (P_{cr}) and ultimate load (P_u) together with their corresponding mid-height lateral displacements (Δ_{cr} and Δ_u, respectively), and the mode of failure are presented in Table 3. Fig. 7 presents the failure pattern of the control specimen C_o, while Fig. 8 presents the failure modes of the slender columns with ECC/SHCC connection. Generally, all the tested columns failed due to the global buckling associated with the buckling of reinforcement bars and concrete crushing. The appearance of the first cracking in the tested columns was delayed as the embedded length of the steel bars increased. This increased the cracking load. It can be observed from Table 3 that increasing the embedded length from 15D to 22.5D, and 30D in columns with ECC in Group G3 increased the cracking load by 10%, and 13%, respectively. Similarly, for columns with SHCC in Group G3, the

Table 2
Mix proportions and compressive strength of the normal concrete, ECC and SHCC.

Concrete	Cement (kg/m^3)	Fine aggregate (kg/m^3)	Coarse aggregate (kg/m^3)	Fly ash (kg/m^3)	Water/binder	Polypropylene Fiber (%) in volume	HRWR (kg/m^3)	f_c' (MPa)	Poions Ratio
NC	350	700	1150	—	0.42	—	—	25.17	0.20
ECC	549	429	—	561	0.28	2.00	14.45	44.19	0.22
SHCC	483	523	—	583	0.29	2.00	9.95	53.40	0.22

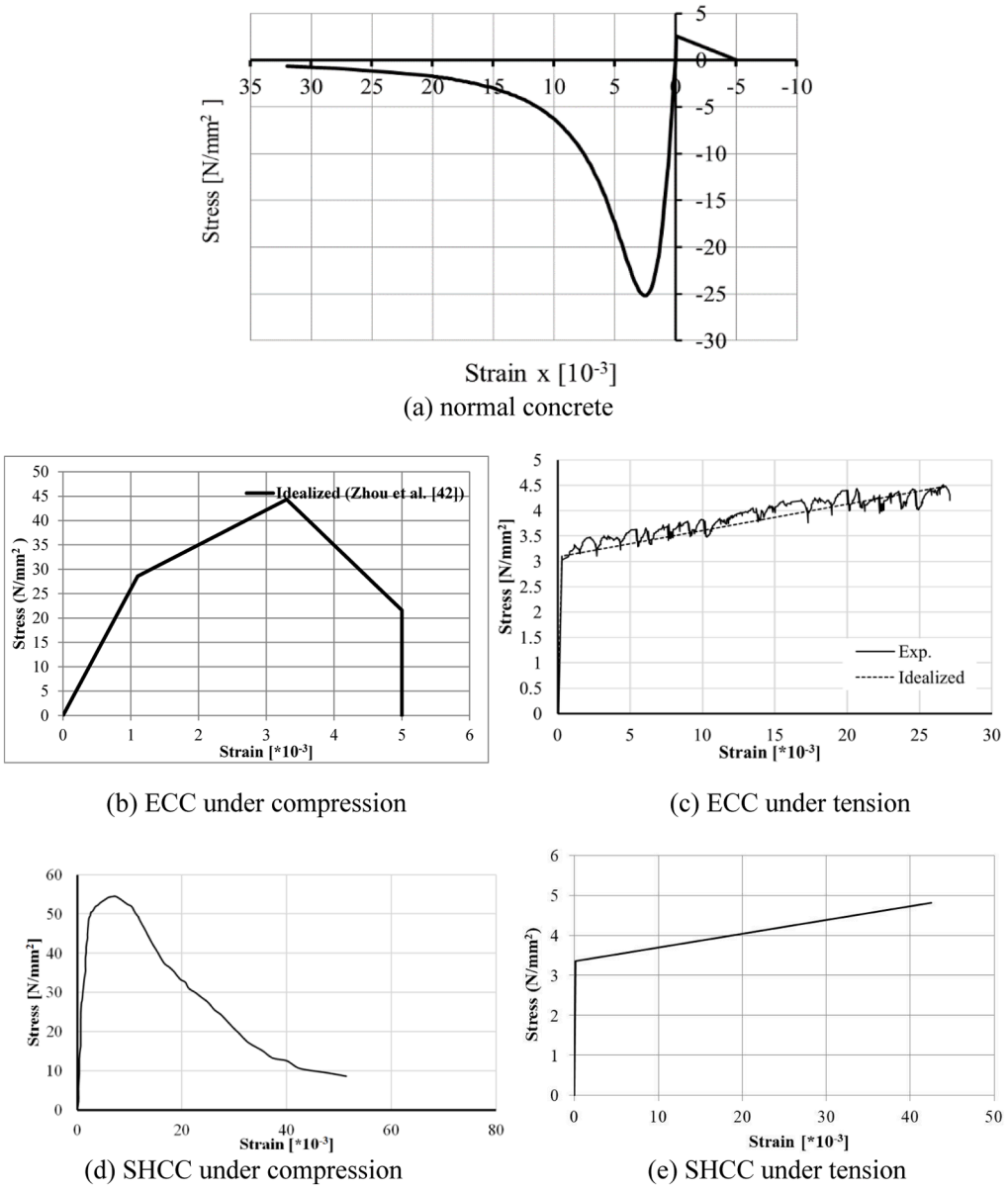

Fig. 4. Constitutive stress–strain laws for different concrete.

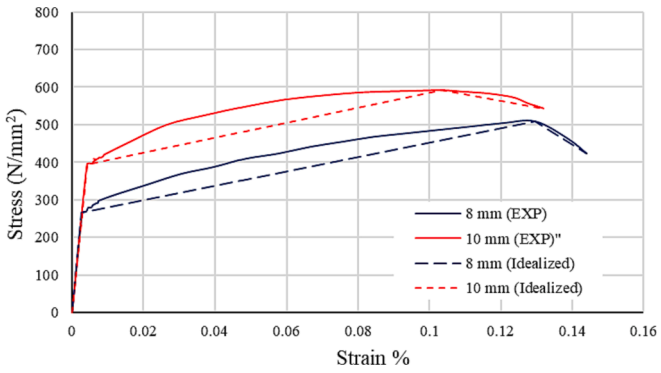

Fig. 5. Actual and idealized uniaxial Stress–strain relationships steel bars.

cracking load increased by 10%, and 11%, respectively. Moreover, increasing the reinforcement ratio further delayed the appearance of the first crack in the tested columns. The columns with ECC/SHCC had higher cracking loads than the control specimen. For example, for column E-0.031-15D and H-0.031-15D, the first crack appeared at the load value of 308.36 kN and 337.86 kN, respectively. However, the cracking load of the column C_o. was 256 kN. This was due to the excellent strain-hardening performance of ECC and SHCC.

Generally, cracks appeared around the mid-length of the columns. As the load increased, the columns buckled globally, and more cracks appeared at the tensile zone at the mid-length of the columns. With further load increment, the concrete in the intermediate connections crushed and the buckled reinforcement bars were exposed as shown in Fig. 8. The columns in Group G3 had lesser lateral displacement at the cracking load compared to the columns in Group G2. For example, columns H-0.036-15D, H-0.036–22.5D, and H-0.036-30D had the lateral displacement about 3.2%, 5.1%, and 9.5% smaller than columns E-0.031–15, E-0.031–22.5, and E-0.031–30, respectively. However, columns with ECC connection had smaller lateral displacement than the columns with SHCC. For example, columns E-0.036-15D, E-0.036–22.5D, and E-0.036-30D had the lateral displacement about 28%, 19%, and 47% smaller than columns E-0.031-15D, E-0.031–22.5D, and E-0.031-30D, respectively as shown in Table 3.

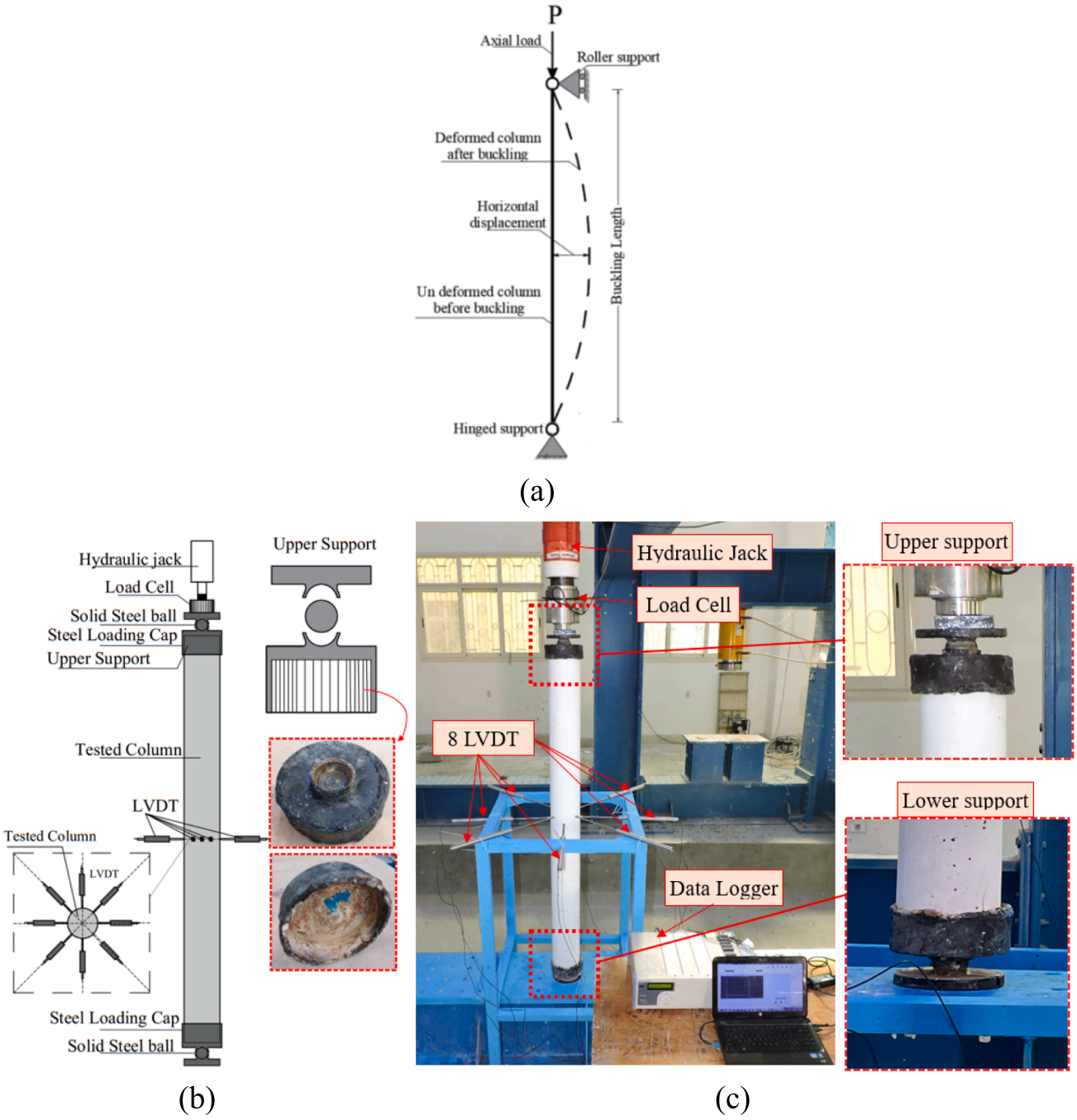

Fig. 6. Test set-up and details of the instrumentations: (a) The structural simulation and boundary condition (b) Schematic view, and (c) Actual test setup.

Fig. 8 shows that the embedded length of steel bars/ intermediate connection can significantly affect the mode of failure for columns. Generally, slender columns with the L_e of 15D failed by the global buckling with damage at the ECC/SHCC connection. On the contrary, the concrete crushing occurred away from the splice in columns with connection lengths of 22.5D, and 30D. This suggests that the splice length should not be less than 22.5D to prevent connection failure.

3.2. Load-horizontal displacement relationship and elastic stiffness

The recorded load-lateral displacement relationships of tested columns are plotted in Fig. 9. Table 3 presents the lateral displacement recorded at the cracking and ultimate loads. Also, the elastic stiffness (k) of columns, which is defined as the slope of the linear performance of load-lateral displacement response, can be found in Table 3. Generally, all tested columns presented linear performance up to the cracking stage. The elastic load values were found to be increased and affected by the length of the ECC/SHCC connection. Increasing the length of the ECC/SHCC connection resulted in higher elastic loads of the tested columns. However, a remarkable increase in elastic load values was recorded for columns having a reinforcement ratio of 0.036 as observed by the third group shown in Fig. 9 (c) and (f). Then, all columns entered the plastic zone with a hardening behavior followed by softening performance up to failure.

Table 3 illustrates that all slender columns with ECC/SHCC connection had a higher elastic stiffness than the control specimen. The elastic stiffness of columns E-0.027-15D, E-0.027–22.5D, and E-0.027-30D is 17%, 28%, and 36% higher than the control specimen,

Table 3
Test results of the circular columns.

Group	Specimen's ID	Cracking Stage			Ultimate Stage			Elastic Stiffness Index (K)	K_C/K_0	Absorbed Energy (E)	Failure mode*
		P_{cr} (kN)	P_{crC}/P_{crB0}	Δ_{cr} (mm)	P_u (kN)	P_{uC}/P_{uC0}	Δ_{Pu} (mm)				
ECC Group											
G1-ECC	C0	256.10	1.00	2.30	444.00	1.00	5.50	111.35	1.00	2574.01	B
	E-0.027–15	234.12	0.91	1.79	469.21	1.06	5.51	130.79	1.17	3505.12	B + C at ECC joint
	E-0.027–22.5	244.25	0.95	1.72	488.25	1.10	5.82	142.01	1.28	4451.23	C at NC Panel
	E-0.027–30	259.11	1.01	1.71	519.36	1.17	4.73	151.53	1.36	4058.60	C at interface
G2-ECC	C0	256.10	1.00	2.30	444.00	1.00	5.50	111.35	1.00	2574.01	B
	E-0.031–15	308.36	1.20	2.22	530.81	1.20	4.50	138.90	1.25	3092.89	B + C at ECC joint
	E-0.031–22.5	319.52	1.25	2.29	549.02	1.24	4.95	139.5	1.26	3678.85	B + C at interface
	E-0.031–30	370.02	1.44	2.68	587.92	1.32	5.66	138.07	1.24	4308.65	B + C at NC Panel
G3-ECC	C0	256.10	1.00	2.30	444.00	1.00	5.50	111.35	1.00	2574.01	B
	E-0.036–15	405.26	1.58	1.73	610.26	1.37	4.45	234.25	2.10	3670.89	B + C at ECC joint
	E-0.036–22.5	447.35	1.75	1.93	642.39	1.45	4.32	231.79	2.08	5325.12	B + C at NC Panel
	E-0.036–30	506.21	1.98	1.82	681.08	1.53	4.88	278.14	2.50	5270.88	B + C at interface surface
SHCC Group											
G1-SHCC	C0	256.10	1.00	2.30	444.00	1.00	5.50	111.35	1.00	2574.01	B
	H-0.027-15D	310.64	1.21	2.29	535.20	1.21	5.21	135.65	1.22	2243.23	B + C at SHCC joint
	H-0.027–22.5D	323.45	1.26	2.26	570.08	1.28	5.37	143.12	1.29	2627.08	B + C at NC Panel
	H-0.027-30D	342.22	1.34	2.21	588.05	1.32	5.43	154.85	1.39	3105.13	B + C at NC Panel
G2-SHCC	C0	256.10	1.00	2.30	444.00	1.00	5.50	111.35	1.00	2574.01	B
	H-0.031-15D	337.86	1.32	2.25	585.54	1.32	5.73	150.16	1.35	3134.22	B + C at SHCC joint
	H-0.031–22.5D	372.47	1.45	2.27	605.72	1.36	5.69	164.08	1.47	3468.70	B + C at NC Panel
	H-0.031-30D	382.57	1.49	2.20	638.33	1.44	5.72	173.89	1.56	3871.54	B + C NC Panel
G3-SHCC	C0	256.10	1.00	2.30	444.00	1.00	5.50	111.35	1.00	2574.01	B
	H-0.036-15D	390.13	1.52	2.18	628.17	1.41	6.68	178.96	1.61	4288.53	B + C at SHCC joint
	H-0.036–22.5D	414.48	1.62	2.16	658.68	1.48	6.69	191.89	1.72	4523.53	B + C at NC Panel
	H-0.036-30D	430.98	1.68	2.01	682.95	1.54	6.71	214.42	1.93	6130.06	B + C at Interface

P_{cr}: Load at which the first crack appeared; **Δ_{cr}**: Horizontal displacement recorded at P_{cr}; **P_u**: Ultimate load; **Δ_{Pu}**: Horizontal displacement recorded at P_U; **K**: elastic index; **E**: Absorbed energy; *Failure mode: **B**: buckling; **C** concrete crushing with steel buckling.

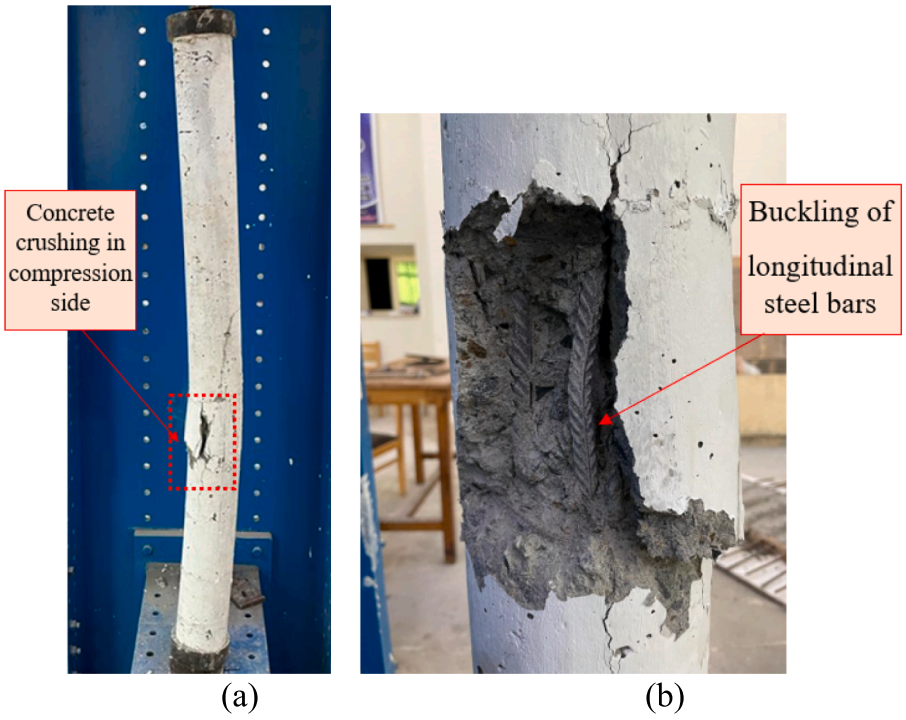

Fig. 7. Failure modes of NC master column (C_0): (a) Concrete crushing caused by column buckling and (b) Buckling of steel bars.

respectively. Similarly, the elastic stiffness of columns H-0.027-15D, H-0.027–22.5D, and H-0.027-30D is 22%, 29%, and 39% higher than the control specimen, respectively. Increasing the reinforcement ratio further increases the elastic stiffness of the columns. For example, the elastic stiffness of columns E-0.036-15D, E-0.036–22.5D, and E-0.036-30D is 110%, 108%, and 150% higher than the control specimen,

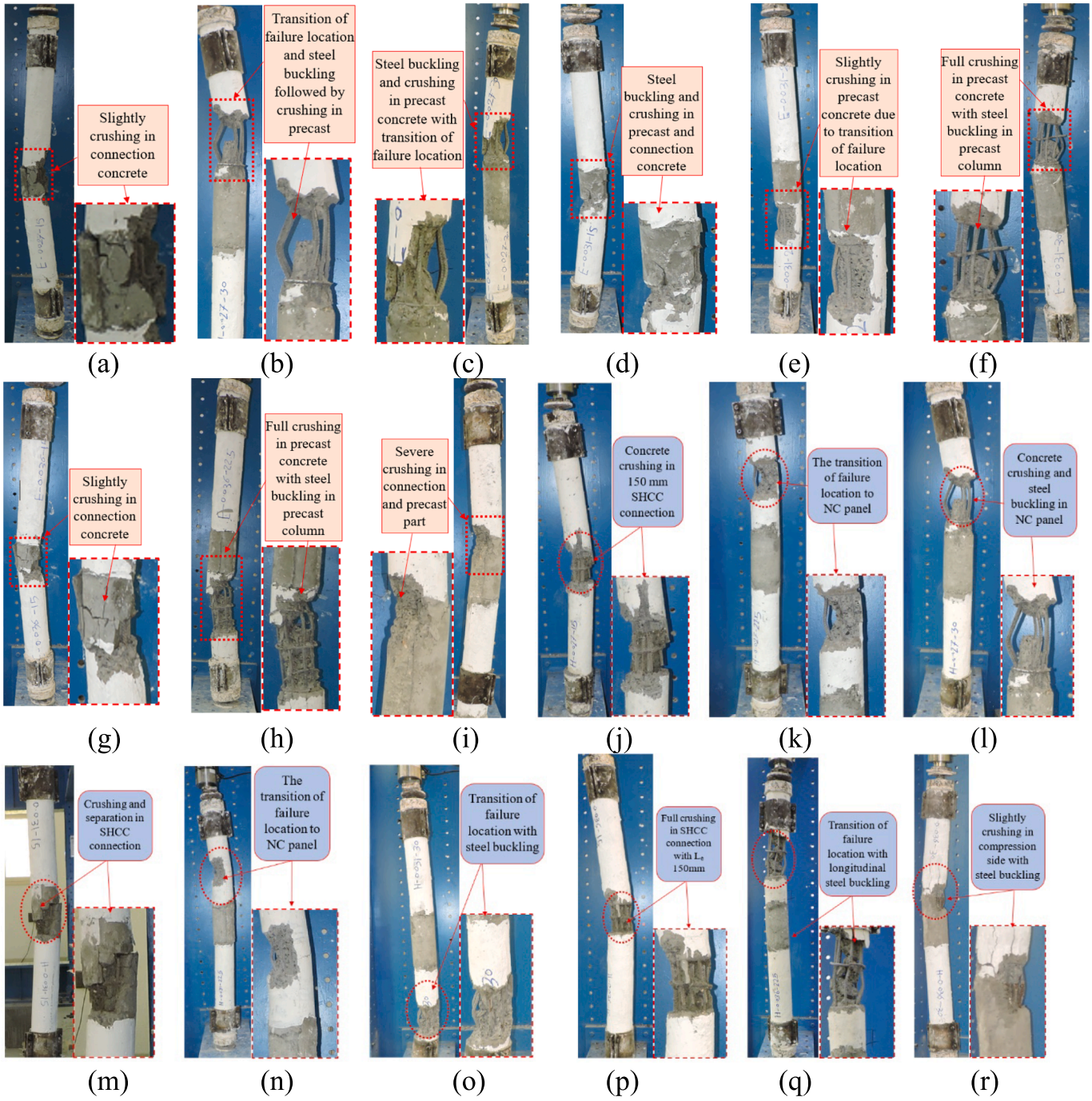

Fig. 8. Failure modes of columns (a) E-0.027–15, (b) E-0.027–22.5, (c) E-0.027–30, (d) E-0.031–15, (e) E-0.031–22.5, (f) E-0.031–30, (g) E-0.036–15, (h) E-0.036–22.5, (i) E-0.036–30, (j) H-0.027-15D, (k) H-0.027–22.5D, (l) H-0.027-30D, (m) H-0.031-15D, (n) H-0.031–22.5D, (o) H-0.031-30D, (p) H-0.036-15D, (q) H-0.036–22.5D, and (r) H-0.036-30D.

respectively. Similarly, the elastic stiffness of columns H-0.036-15D, H-0.036–22.5D, and H-0.036-30D is 61%, 72% and 93% higher than that of the control specimen, respectively.

3.3. Capacity of absorbed energy

As an indication of the ductility performance, the absorbed energy (E) of the tested columns was estimated as the total area under the load-lateral displacement recorded during the test [31,32]. Table 3 compares the E values calculated for all tested columns. The superior features of strain-hardening and tension-stiffening associated with ECC/SHCC reflected a better and significant improvement to the energy absorption of the columns when compared to the control specimen. For instance, for the same L_e of 15D, the energy absorbed capacity of the columns with ECC connection and a reinforcement ratio of 0.027, 0.031 and 0.036 is found to be 36%, 20%, and 43% higher than that of the control specimen, respectively as shown in Table 3. Similarly, for columns with L_e = 22.5D, the increase in the energy absorbed capacity is 73%, 43%, and 107%, respectively compared to the control specimen. Accordingly, when L_e is 30D, the increase in the energy absorption for columns with ECC and the reinforcement ratio of 0.027, 0.031, and 0.036 is 58%, 67%, and 105%, respectively when compared to the control specimen, as shown in Table 3. Similarly, for columns with SHCC connection and L_e of 30D, the increase in the energy absorption for columns with a

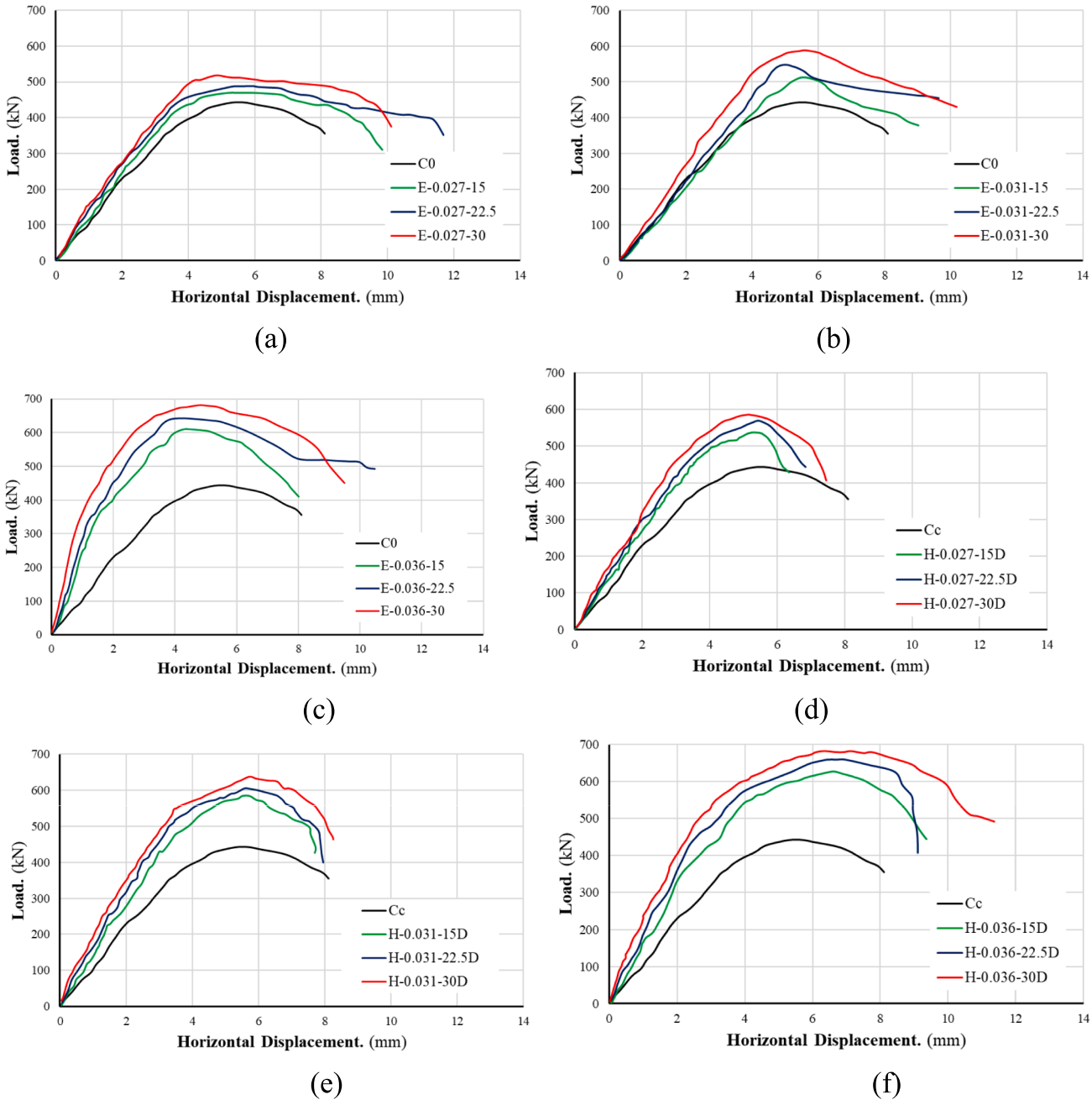

Fig. 9. Load-displacement relationships for tested columns of Group: (a) G1-ECC, (b) G2-ECC, (c) G3-ECC, (d) G1-SHCC, (e) G2-SHCC, (f) G3-SHCC.

reinforcement ratio of 0.027, 0.031, and 0.036 is 21%, 50%, and 138%, respectively when compared to the control specimen.

3.4. Cracking and ultimate loads

Table 3 presents the cracking and ultimate loads of the tested columns. The cracking load of columns with ECC/SHCC connection is higher than that of the control specimens except for the columns with ECC in Group G1. For example, for specimens E-0.031-15D, E-0.031–22.5D, and E-0.031-30D, the cracking load is 20%, 25% and 44% higher than that of the specimen $C_{0,}$ respectively. Similarly, the cracking load of the columns E-0.036-15D, E-0.036–22.5D, and E-0.036-30D is 58%, 75%, and 98% higher than that of specimen C_0. For columns with SHCC connection, the cracking load of the columns H-0.036-15D, H-0.036–22.5D, and H-0.036-3D0 is 52%, 62%, and 68% higher than that of specimen C_0. For the same embedded length of steel bars/ intermediate concrete connection of the column, increasing the reinforcement ratio generally increases the cracking load of the columns. For example, the cracking of columns E-0.031–22.5 is 24% higher than that of the column E-0.027–22.5. Similarly, the cracking load of column E-0.036–22.5 is 29% higher than that of column E-0.031–22.5. The appearance of the first cracking load was delayed as the reinforcement ratio of the column increased. For instance, the cracking load of E-0.036–15, E-0.036–22.5, and E-0.036–30 is 66%, 70%, and 74% of their ultimate load, respectively. On the contrary, the cracking load of columns in Group G2, E-0.031–15, E-0.031–22.5, and E-0.031–30 is 58%, 58%, and 63% of their ultimate load, respectively.

Test results show that the ultimate load of all tested columns with an ECC/SHCC connection is higher than that of the control specimen. The ultimate load of specimens E-0.027–15, E-0.027–22.5, and E-0.027–30

is 6%, 10%, and 17% higher than that of specimen C_0. Similarly, for specimens E-0.031–15, E-0.031–22.5, and E-0.031–30, the ultimate load is 20%, 24%, and 32% higher than that of specimen C_0. For specimens in Group G3 with ECC connection, the ultimate load of E-0.036–15, E-0.036–22.5, and E-0.036–30 is 37%, 45%, and 53% higher than that of specimen C_0. Similar results are observed for columns with SHCC connection. For the same reinforcement ratio, increasing the embedded length increases the ultimate load of the columns. For instance, the ultimate load of column E-0.036–15 is 13% higher than that of column E-0.031–15 whereas the ultimate load of column E-0.031–15 is 12% higher than that of column E-0.027–15. For columns with an embedded length of 22.5D, increasing the reinforcement ratio from 0.027 to 0.031 and 0.036 increases the ultimate load of the column by 11% and 15%, respectively. Similarly, for columns with an embedded length of 30D, the increase in the ultimate load for columns in Groups G2 and G3 is 12% and 14% higher than that of the column in Group G1. Similar results are observed for columns with SHCC connection.

4. Numerical simulation

Numerical models were developed utilizing the ABAQUS software [33]. The development of the FE models is described in detail in the following sections.

4.1. Material constitutive modeling and analysis of sensitive numerical parameters

The concrete damage plasticity (CDP) model in the ABAQUS program was employed to model the concrete parts. The CDP was used to simulate the elastic–plastic behavior of concrete under tension and compression as well as the deterioration caused by cracking [34,35]. Several attempts were performed to study the sensitivities of variables in the CDP model, including dilation angle (ψ), flow potential eccentricity (e), the ratio of biaxial to uniaxial compressive stresses (f_{bo}/f_{co}), the ratio of the second stress invariant on the tensile to compressive meridian (K_c), and viscosity relaxation parameter (μ). After several trials, ψ was selected as 28° and 35° for NC and ECC/SHCC, which were very close to the ones reported previously [36,37]. The flow potential eccentricity appeared to have an insignificant influence on the performance; therefore, the current model used the defaulted value of $e = 0.1$ for NC and ECC/SHCC. The ratio of f_{bo}/f_{co} varied from 1.10 to 1.16 as suggested in previous studies [38,39]; however, the value of 1.16 provided acceptable results and thus was adopted in this study. The K_c value is commonly considered within the range of 0.64 to 0.80; however, a good accuracy was obtained for the value of $k_c = 0.66$. A similar value was also used by the authors previously [40]. Several models were run with various μ values starting from 0.00 to 0.001. However, previous studies [36,41] recommended that $\mu = 0.00$ gave satisfactory solutions so that it was adopted in this study. The idealized stress–strain relationships of NC and ECC/SHCC under compression and tension, as shown in Fig. 4 were used in the numerical modeling. Zhou et al. [42] proposed the idealized stress–strain relationships of ECC shown in Fig. 4. The idealized stress–strain relationships of steel bars shown in Fig. 5 were used to simulate the performance of steel bars. The Poisson's ratio of steel was taken as 0.3 and Young's modulus was taken as 200 GPa.

4.2. Model set-up, meshing, and interaction

An eight-node linear hexahedral solid element with reduced integration (C3D8R), was selected to model NC, ECC/SHCC, and rigid supporting/loading steel plates as shown in Fig. 10. The steel rebars were modeled utilizing the two-node and linear truss element (T3D2). The sensitive analysis has been performed with mesh size varied from 35 mm to 20 mm; however, the size of 25 mm resulted in satisfactory solutions with lower computational cost. A full bond was assumed between the steel bars and the concrete. Embedded interaction was adopted for steel bars and concrete parts. The concrete column was defined as the host zone while the bar truss elements were known as the embedded elements. A rigid circular cap as shown in Fig. 10 was used to apply the load and as support. The top end of the column was simulated as a roller support allowing vertical movement, while the bottom end was modeled as a pinned support, as shown in Fig. 10c.

The interaction between reinforcing steel bars embedded in the ECC/SHCC connection was modeled using the Eligehausen technique [43]. A

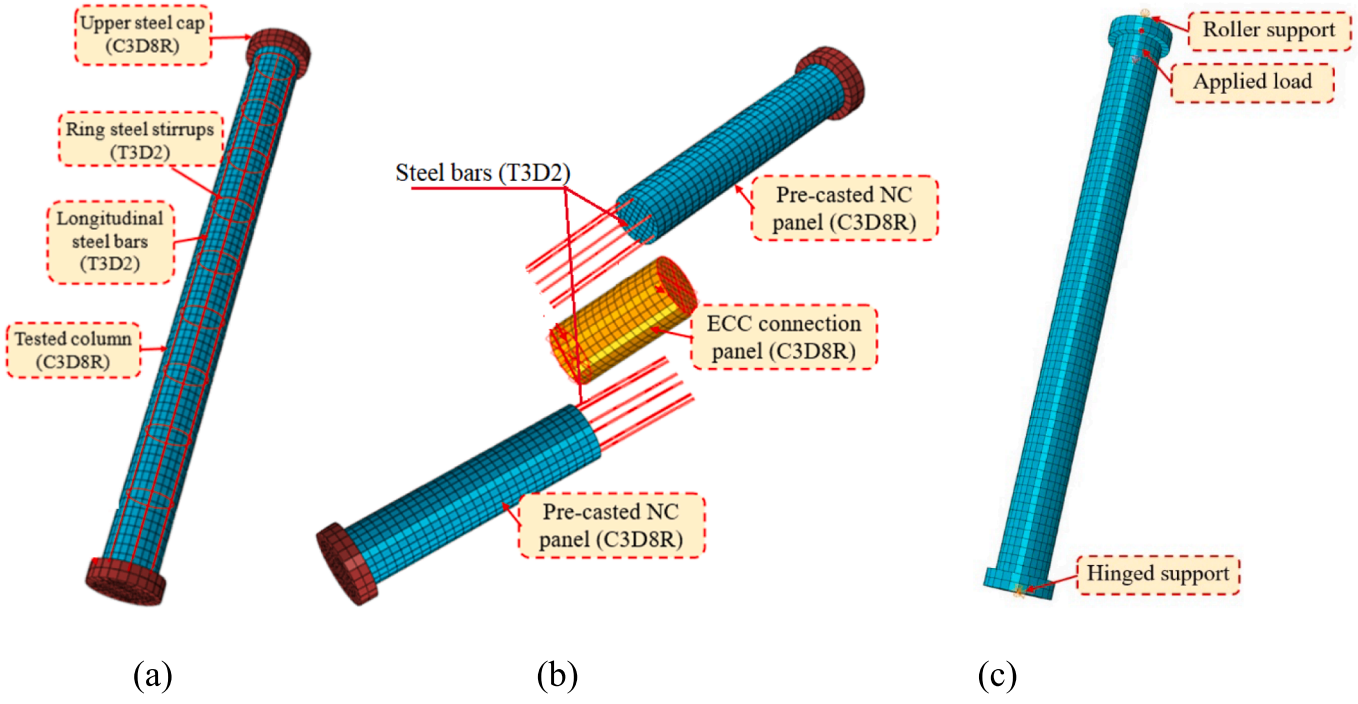

Fig. 10. Model set-up and element types: (a) Solid NC, (b) precast column with ECC/SHCC connection, and (c) boundary conditions.

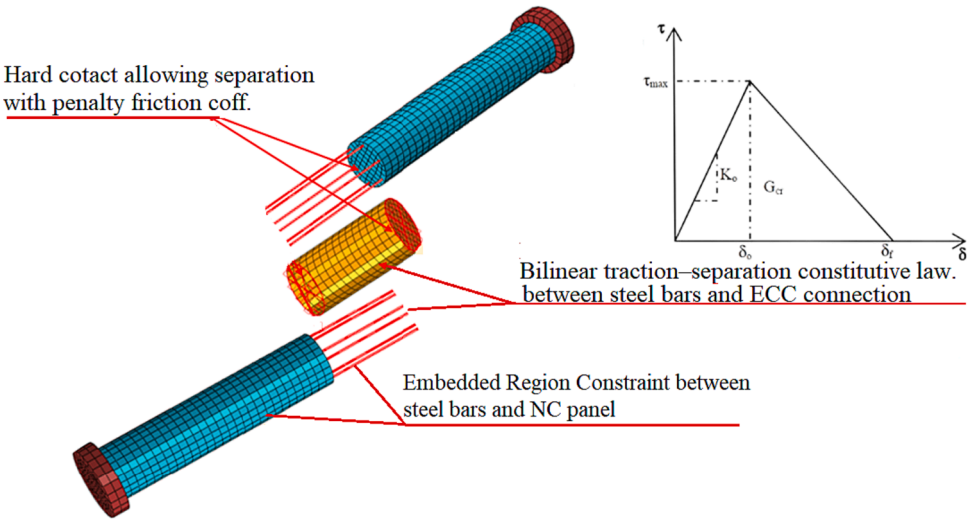

Fig. 11. Model interactions.

cohesive-damage interaction is exhibited as simple bilinear traction–separation law defined in terms of effective traction τ and effective opening displacement δ. Fig. 11 shows the relationship between the traction stress and effective opening displacement, defined by the stiffness (K_0), the local bond strength of concrete (τ_{max}), a characteristic opening displacement at fracture (δ_f), and the energy needed for opening the crack (G_{cr}) which is equal to the area under the traction–displacement curve.

As shown in Fig. 11, the interaction between ECC/SHCC intermediate connection and the two precast NC panels was modeled using hard contact between the two surfaces [44]. This assumption was reached by considering the outer circular surfaces of the ECC/SHCC connection to be the slave while the other opposite circular NC surfaces were set to be the master. This interaction strategy was modeled to allow separation with a penalty friction coefficient of 0.6.

4.3. Initial imperfection of the columns

PC slender columns usually have initial imperfections which may be due to geometric details, pre-fabrication or boundary imperfections [45–49]. Several simulations were performed with different additional eccentricities arising from initial imperfection ($e_{i,m}$). These initial imperfections at the mid-height of the column were taken as L/1000, L/900, L/800, L/700, L/600, L/500, and L/400, where L is the column length (1700 mm). The simulated load-lateral displacement curves with various initial imperfections are shown in Fig. 12. The figure demonstrates that the use of an initial imperfection of L/400 yields acceptable ultimate capacity and load lateral-displacement response.

4.4. Numerical results and verifications

The reliability of the developed FEM was validated by comparing the numerical simulations with experimentally recorded results including load-lateral displacement curves, failure modes, and both loads recorded at first cracking and ultimate stages. Both cracking and ultimate loads observed experimentally and numerically together with their corresponding lateral displacements are provided in Table 4. It appears from Table 4 that the cracking and ultimate loads obtained by FEM agree well with experimental data. The average value of $P_{cr\ FE}/P_{cr\ EXP}$ ratios for columns with ECC connection is about 1.06, 0.95, and 0.96 for Groups G1, G2, and G3, respectively with a standard deviation (SD) of about 0.01 for all groups. Similarly, for columns with SHCC connection, the average value of $P_{cr\ FE}/P_{cr\ EXP}$ ratios is about 1.05, 1.05, and 1.05 for Groups G1, G2, and G3, respectively. Moreover, the average value of P_{uFE}/P_{uEXP} is about 1.06, 1.03, and 1.03, respectively for columns in Groups G1, G2, and G3 with ECC connection where, the average value of P_{uFE}/P_{uEXP} is about 1.01, 1.02, and 1.02, respectively for columns in Groups G1, G2, and G3 with SHCC connection. Furthermore, the comparisons of the predicted and experimentally recorded lateral displacement recorded at cracking load and ultimate load are presented in Table 4 where an excellent match between the test and FEM prediction is observed.

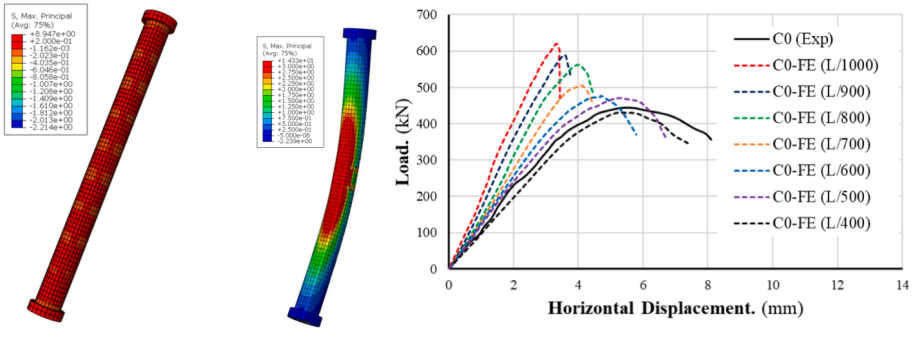

Fig. 12. Effect of eccentricities for initial imperfection; (a) Pure compression tresses visualized for slender column loaded axially without eccentricity; (b) Stresses visualized for slender column loaded axially with eccentricity; (c) Load-lateral displacement.

Table 4
Comparison between numerical and experimental results.

Specimen ID	P_{cr} (kN)			Δ_{cr} (mm)			P_u (kN)			Δ_{Pu} (mm)		
	EXP.	**FE**	**FE/ EXP**	**EXP.**	**FE**	**FE/ EXP**	**EXP**	**FE**	**FE/ PEX**	**EXP**	**FE**	**FE/ EXP**
ECC group												
E-0.027–15	234.1	251.00	1.07	1.79	1.71	0.96	469.2	492.10	1.05	5.51	5.41	0.98
E-0.027–22.5	244.2	256.30	1.05	1.72	1.69	0.98	488.2	521.30	1.07	5.82	5.63	0.97
E-0.027–30	259.1	272.80	1.05	1.71	1.68	0.98	519.3	554.60	1.07	4.73	4.65	0.98
Avg			1.06			0.97			1.06			0.98
SD			0.01			0.02			0.01			0.01
COV			0.00014			0.00024			0.00012			0.00007
E-0.031–15	308.3	289.20	0.94	2.22	2.04	0.92	530.8	542.90	1.02	5.50	5.41	0.98
E-0.031–22.5	319.5	303.40	0.95	2.41	2.32	0.96	549.0	568.30	1.04	4.95	4.81	0.97
E-0.031–30	370.0	356.80	0.96	2.68	2.61	0.97	587.9	615.30	1.05	5.66	5.32	0.94
Avg			0.95			0.95			1.03			0.97
SD			0.01			0.03			0.01			0.02
COV			0.00017			0.00084			0.00014			0.0051
E-0.036–15	405.2	389.80	0.96	1.73	1.65	0.95	610.2	629.30	1.03	4.45	4.32	0.97
E-0.036–22.5	447.3	432.50	0.97	1.93	1.86	0.96	642.3	666.87	1.04	4.32	4.16	0.96
E-0.036–30	506.2	480.60	0.95	1.82	1.73	0.95	681.0	700.10	1.03	4.88	4.68	0.96
Avg			0.96			0.96			1.03			0.96
SD			0.01			0.01			0.01			0.01
COV			0.0008			0.0004			0.0002			0.0003
SHCC group												
H-0.027-15D	310.64	329.23	1.06	2.29	2.26	0.99	535.2	546.95	1.02	5.21	5.18	0.99
H-0.027–22.5D	323.45	340.11	1.05	2.26	2.22	0.98	570.08	576.08	1.01	5.37	5.25	0.98
H-0.027-30D	342.22	366.13	1.07	2.21	2.15	0.97	588.05	602.07	1.02	5.43	5.28	0.97
Avg			1.05			0.98			1.01			0.98
SD			0.01			0.01			0.02			0.01
COV			0.0048			0.0022			0.0052			0.0034
H-0.031-15D	337.86	355.45	1.05	2.25	2.23	0.99	585.54	595.02	1.02	5.73	5.62	0.98
H-0.031–22.5D	372.47	384.27	1.03	2.27	2.21	0.97	605.72	620.24	1.02	5.69	5.36	0.94
H-0.031-30D	382.57	404.24	1.06	2.20	2.10	0.95	638.33	654.36	1.03	5.72	5.67	0.99
Avg			1.05			0.97			1.02			0.97
SD			0.01			0.02			0.01			0.03
COV			0.0066			0.0091			0.0024			0.0130
H-0.036-15D	390.13	403.98	1.04	2.18	2.17	1.00	628.17	643.35	1.02	6.68	6.65	1.00
H-0.036–22.5D	414.48	434.85	1.05	2.16	2.15	1.00	658.68	671.07	1.02	6.69	6.54	0.98
H-0.036-30D	430.98	446.69	1.04	2.01	1.95	0.97	682.95	694.97	1.02	6.71	6.68	1.00
Avg			1.04			0.99			1.02			0.99
SD			0.01			0.02			0.00			0.01
COV			0.0038			0.0073			0.0017			0.0052

EX: Experimental; **FE**: Finite Element Model; **Avg:** Average; **SD:** Standard deviation; **COV:** Coefficient of variation.

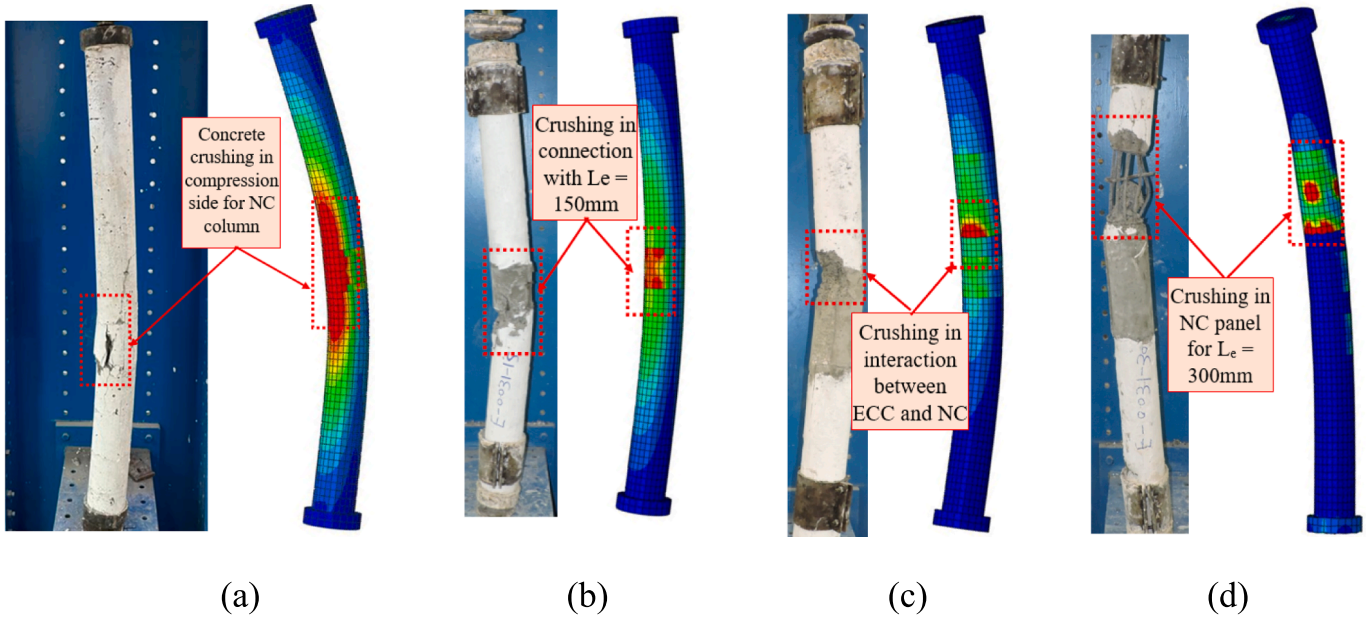

Fig. 13. Crack pattern and stresses distribution: (a) for NC master column C_0, (b) column with ECC connection and $L_e = 15D$, (c) column with ECC connection and $L_e = 22.5D$, and (d)) column with ECC connection and $L_e = 30D$.

The failure modes predicted by FEM are compared with the test observations in Fig. 13. A good match can be observed. It is seen from Figs. 8 and 13 that the columns with the embedded length of 15D failed at their mid-height whereas the failure of columns with the embedded length of 22.5D and 30D generally occurred at places away from the splices. For the master column C_0, the initial crack appeared around its mid-height but extended towards the bottom and failed due to the overall buckling. It appears that the FE model can accurately predict the failure location of the tested columns. The difference between the FE and test results in terms of failure could be due to the uncertainty of the initial imperfections of the tested columns which were not measured during the test. However, the sensitivity analyses of the initial geometric imperfections were undertaken to best match the test results.

The load-lateral displacement relationships predicted numerically together with those recorded experimentally are compared in Fig. 14. It can be found from Fig. 14 that the FEM simulates well the experimentally measured load-lateral displacement curves of RC slender columns.

5. Conclusions

This study has investigated experimentally and numerically the structural performance of circular PC slender columns with splice connection filled with ECC/SHCC subjected to compressive loading. The effects of the reinforcement ratio and the embedded length on the

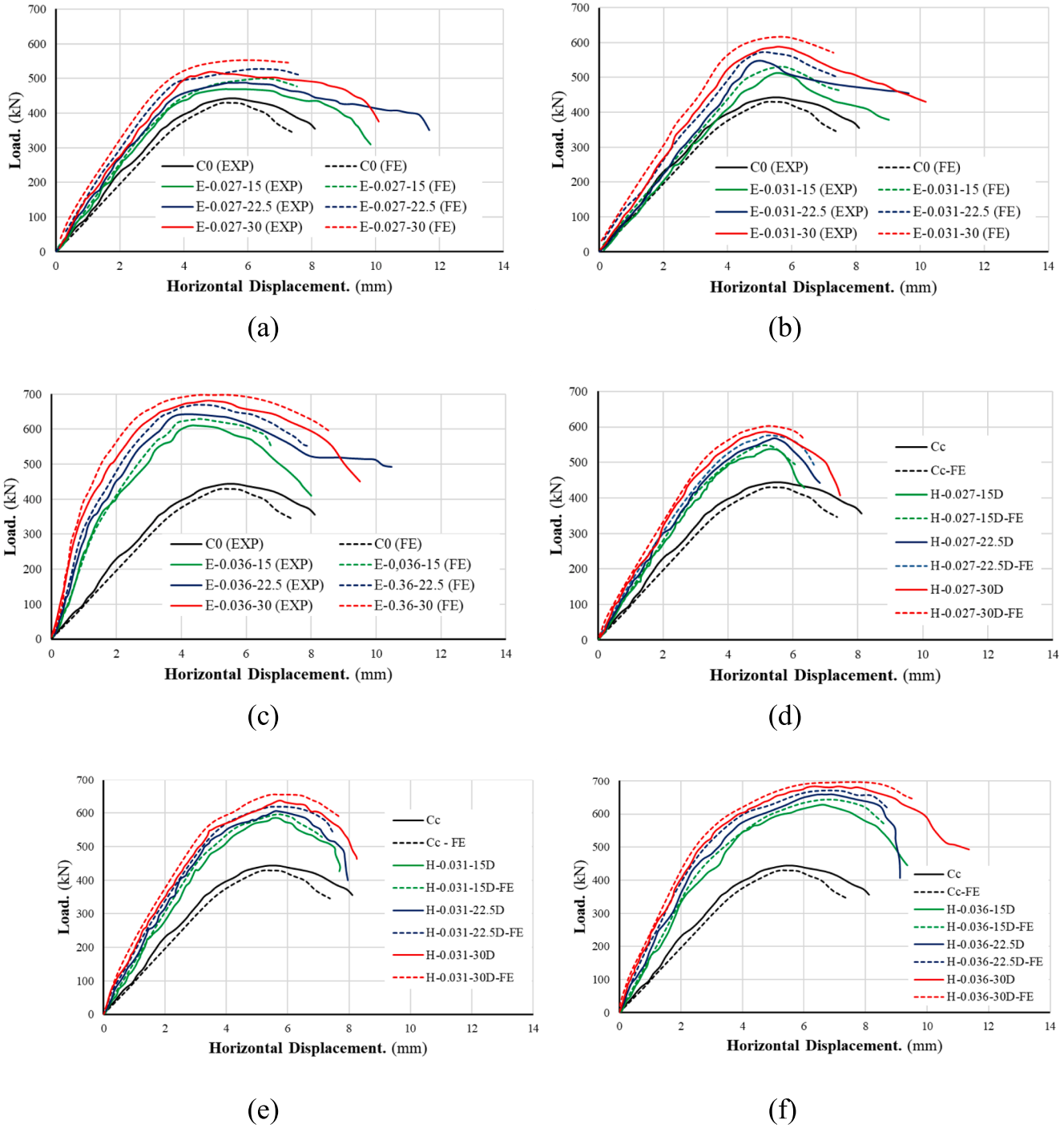

Fig. 14. Load-displacement responses obtained experimentally and numerically: (a) G1-ECC, (b) G2-ECC, (c) G3-ECC, (d) G1-SHCC, (e) G2-SHCC, (f) G3-SHCC.

responses of PC slender columns with splices have been ascertained. Three-dimensional nonlinear FEM was developed using ABAQUS to simulate the performance of such columns.

Based on the experimental and numerical results, the following conclusions could be drawn:

1. The common failure of the tested columns was the global buckling associated with concrete crushing. Increasing the embedded length of the steel bars/splice connections and reinforcement ratio delayed the appearance of the first crack in the tested columns. Moreover, the columns with L_e of 15D failed at the ECC/SHCC connection while increasing L_e resulted in the transformation of the failure zone away from the splice.
2. All the tested columns with ECC/SHCC connections had a higher elastic stiffness than the control specimen. Increasing the reinforcement ratio and the embedded length of the steel bars/ECC connections increases the elastic stiffness of the columns. The elastic stiffness of columns with ECC and SHCC connection increased by 150% and 93%, respectively when compared to the control specimen.
3. Filling the splices with ECC and SHCC increased the energy absorption capacity of the columns by 150% and 138%, respectively in comparison with the control specimen.
4. Increasing the reinforcement ratio from 0.027 to 0 0.036 increased the energy absorption capacity of the columns with SHCC and the splice length of 15D and 30D by 91% and 97%, respectively.
5. The developed FEM predicts well the experimentally measured performance of circular PC slender columns with ECC/SHCC connection. Therefore, the FEM can be employed to undertake future parametric studies.

Due to the different concrete mix designs used for the different concrete, the strength of the concrete used in the column splices was different from each other. The most economical way is to use the FE model to investigate the performance of PC slender columns made of different concrete with the same compressive strength. Further study on the effects of concrete strength on the response of PC columns with splices should be undertaken using the validated FE model.

Declaration of Competing Interest

The authors declare that they have no known competing financial interests or personal relationships that could have appeared to influence the work reported in this paper.

Acknowledgments

The help from technicians at Kafrelsheikh University in performing the tests is acknowledged. Part of the experimental program is funded by the first author. This research is also supported by the Researchers Supporting Project number (RSP2023R343) provided by King Saud University, Riyadh, Saudi Arabia.

References

[1] Yee AA, Eng PHD. Social and environmental benefits of precast concrete technology. PCI J 2001;46(3):14–9.
[2] Xu C, Chen Da, Miramini S, Liu X, Xu W, Zhang L. Experimental fire performance assessment of a new type of prestressed composite circular precast concrete columns. Eng Struct 2023;278:115509.
[3] Lynn AC, Moehle JP, Mahin SA, Holmes WT. Seismic evaluation of existing reinforced concrete building columns. Earthq Spectra 1996;12(4):715–39.
[4] Saatcioglu M, Ozcebe G. Response of reinforced concrete columns to simulated seismic loading. Structural Journal 1989;86(1):3–12.
[5] Elwood KJ, Eberhard MO. Effective Stiffness of Reinforced Concrete Columns. ACI Struct J 2009;106(4).
[6] Ma Y, Che Y, Gong J. Behavior of corrosion damaged circular reinforced concrete columns under cyclic loading. Constr Build Mater 2012;29:548–56.
[7] Abadel AA, Masmoudi R, Khan MI. Axial behavior of square and circular concrete columns confined with CFRP sheets under elevated temperatures: Comparison with welded-wire mesh steel confinement. Structures 2022;45:126–44.
[8] Obaidat AT, Ashteyat AM, Hanandeh S, Al-Btoush AY. Behavior of heat damaged circular reinforced concrete columns repaired using Carbon Fiber Reinforced Polymer rope. J Build Eng 2020;31:101424.
[9] Zhao B, Taucer F, Rossetto T. Field investigation on the performance of building structures during the 12 May 2008 Wenchuan earthquake in China. Eng Struct 2009;31(8):1707–23.
[10] Yang Y, Fang S, Feng W, Wan S, Li L, Tang Y. Flexural and compressive performance of BFRP-reinforced geopolymer sea-sand concrete beams and columns: Experimental and analytical investigation. Compos Struct 2023;318:117089.
[11] Xiao J-L, Nie X, Liu Y-F, Fan J-S. Structural performance assessment of RC flexural members through crack-based fibre beam-column model updating. Comput Struct 2023;281:107029.
[12] Hong Y, Luo Z, Heping Z. Experiments and nonlinear analysis on seismic behavior of RC columns considering buckling and fatigue damage of reinforcing steel bar. J Build Struct 2013;34(11):130.
[13] Robinson GP. Design and performance of precast concrete structures. Loughborough University; 2014.
[14] Beni MT, Madhkhan M. Experimental study on two innovative ductile moment-resisting precast concrete beam-column connections. Structures 2022;39:559–72.
[15] Wei J, Xie Z, Zhang W, Yang Y, Luo X, and Chen B. Axial compressive property of UHPC plate-CFST laced composite columns. Case Studies in Construction Materials 2022;16:e01085.
[16] Zhang Z, Wu X, Sun Q, Tian P, Hu G. Compressive behavior of corroded reinforced concrete columns strengthened with BFRP reinforced ECC in marine environment. Ocean Eng 2023;279:114533.
[17] Lai B-L, Zhang M-Y, Zheng X-F, Chen Z-P, Zheng Y-Y. Experimental study on the axial compressive behaviour of steel reinforced concrete composite columns with stay-in-place ECC jacket. J Build Eng 2023;68:106174.
[18] Dong B, Pan J, Xu Li. Numerical and theoretical analysis of beam-to-column connections with ECC ring beams subjected to local compression loading. J Build Eng 2022;52:104466.
[19] Hung C-C, Hsiao H-J, Shao Yi, Yen C-H. A comparative study on the seismic performance of RC beam-column joints retrofitted by ECC, FRP, and concrete jacketing methods. J Build Eng 2023;64:105691.
[20] Khalil A-E, Atta AM, Hassan A, Abd-Elaaty AH. Flexural strength recovery of RC one-way slabs having cut-outs using NSM-SHCC plates. Eng Struct 2022;258:114149.
[21] Huo Y, Sun H, Chen Z, Yang Y. Mechanical properties and its reliability prediction of engineered/strain-hardening cementitious composites (ECC/SHCC) with different moisture contents at negative temperatures. Cem Concr Compos 2022;134:104812.
[22] Wei J, Liu H, Leung CKY. Application of high-strength strain-hardening cementitious composites (SHCC) in the design of novel inter-module joint. Constr Build Mater 2022;359:129491.
[23] Xu Y, Jia Y, Tong Z, Shivahari S. Cyclic loading test for concrete bridge columns integrated with ECC segment at the plastic zone. Eng Struct 2021;246:112985.
[24] Emara M, Mohamed HA, Rizk MS, Hu JW. Behavior of ECC columns confined using steel wire mesh under axial loading. J Build Eng 2021;43:102809.
[25] Qian H, Ye Y, Yan C, Jin G, Li C, Shi Y. Experimental study on the seismic performance of self-centering bridge piers incorporating ECC and superelastic SMA bars in the plastic hinge regions. Structures 2022;46:1955–67.
[26] Li S, Chan T-M, Young B. Mechanical analysis and finite element modeling of FRP-ECC-HSC composite stub column under axial compression. J Build Eng 2022;62:105212.
[27] Baraghith AT, Khalil A-H-A, Etman EE, Behiry RN. Improving the shear behavior of RC dapped-end beams using precast strain-hardening cementitious composite (P-SHCC) plates. Structures 2023;50:978–97.
[28] Esmaeeli E, He Y. Cast-in-situ vs prefabricated solution based on NSM-CFRP reinforced SHCC for seismic retrofitting of severely damaged substandard RC beam-column joints. J Build Eng 2021;43:103132.
[29] Hamoda A, Ahmed M, Ghalla M, Liang QQ, and Abadel AA. Flexural performance of precast circular reinforced concrete members with intermediate connection filled with ultra-high-performance-concrete. Case Studies in Construction Materials 2023:e02386.
[30] ACI 318-19. Building Code Requirements for Structural Concrete and Commentary. Farmington Hills, Michigan, USA. 2019.
[31] Gopal SR, Manoharan PD. Experimental behaviour of eccentrically loaded slender circular hollow steel columns in-filled with fibre reinforced concrete. J Constr Steel Res 2006;62(5):513–20.
[32] Punurai W, Hsu C-T-T, Punurai S, Chen J. Biaxially loaded RC slender columns strengthened by CFRP composite fabrics. Eng Struct 2013;46:311–21.
[33] Hibbitt K, Sorensen I. "ABAQUS Theory Manual, User Manual and Example Manual," ed: Simulia. RI, USA: Providence; 2000.
[34] Hamoda AA, Eltaly B, and Ghalla MS. Numerical investigation on reinforced concrete closed curved beams subjected to internal pressure strengthened with sustainable material. ERJ. Eng Res J, 2023;.
[35] Elsamak G, Salama MI, Hamoda A. Behavior of Precast Segmental Beams Made of High-strength Concrete and Ultra-high Performance Fiber Concrete Connected by Shear Keys Technique. Arab J Sci Eng 2023;48(4):4907–23.
[36] Hamoda A, Hossain K. Numerical Assessment of Slab-Column Connection Additionally Reinforced with Steel and CFRP Bars. Arab J Sci Eng 2019;44(10):8181–204.

[37] Jahani Y, Baena M, Barris C, Torres L, Sena-Cruz J. Effect of fatigue loading on flexural performance of NSM CFRP-strengthened RC beams under different service temperatures. Eng Struct 2022;273:115119.
[38] Le TT, Patel VI, Liang QQ, Huynh P, Ha NS. Numerical analysis of square concrete-filled double-skin tubular columns with outer stainless-steel tube. Struct Concr 2022;23(5):2968–85.
[39] Yu K, Wang Y, Yu J, Xu S. A strain-hardening cementitious composites with the tensile capacity up to 8%. Constr Build Mater 2017;137:410–9.
[40] Hamoda A, Abdelazeem F, Emara M. Concentric compressive behavior of hybrid concrete–stainless steel double-skin tubular columns incorporating high performance concretes. Thin-Walled Struct 2021;159:107297.
[41] Hamoda A, Ahmed M, Sennah K. Experimental and numerical investigations of the effectiveness of engineered cementitious composites and stainless steel plates in shear strengthening of reinforced concrete beams. Struct Concr 2023;24(2):2778–99.
[42] Zhou J, Pan J, Leung CK. Mechanical behavior of fiber-reinforced engineered cementitious composites in uniaxial compression. J Mater Civ Eng 2015;27(1):04014111.
[43] Eligehausen R, Popov EP, and Bertero VV, "Local bond stress-slip relationships of deformed bars under generalized excitations," Earthquake Engineering Center, University of California, Berkeley, UCB/EERC-83/23, 1982.
[44] El-Mandouh MA, Elsamak G, Rageh BO, Hamoda A, and Abdelazeem F. Experimental and numerical investigation of one-way reinforced concrete slabs using various strengthening systems. Case Stud Construct Mater 2023;18:e01691.
[45] Aristizabal-Ochoa JD. Stability of multi-column systems with initial imperfections and non-linear connections. Int J Non Linear Mech 2013;57:75–89.
[46] Harvey Jr P, Cain T. Buckling of elastic columns with initial imperfections and load eccentricity. Structures 2020;23:660–4.
[47] Liao F-Y, Han L-H, Tao Z. Behaviour of CFST stub columns with initial concrete imperfection: analysis and calculations. Thin-Walled Struct 2013;70:57–69.
[48] Mahmoud KA. Overview of Factors Affecting the Behavior of Reinforced Concrete Columns with Imperfections at High Temperature. Fire Technol 2022;58(2):851–87.
[49] Tomski L, Podgórska-Brzdękiewicz I. Global buckling and the interaction of initial imperfections of columns subjected to conservative loading. Thin-Walled Struct 2011;49(5):596–603.